Applied Biochemistry and Biotechnology (2020) 191:496–510
https://doi.org/10.1007/s12010-019-03181-0

Drug Delivery of Amphotericin B through Core-Shell Composite Based on PLGA/Ag/Fe_3O_4: In Vitro Test

Shiva Sadat Akhavi [1] · Shahram Moradi Dehaghi [1]

Received: 21 August 2019 / Accepted: 11 November 2019 /
Published online: 4 December 2019

Abstract
This research aimed at developing and designing a slow and targeted delivery of Amphotericin B (AmB) antibiotic by placing three types of shells containing different ratios of biodegradable and biocompatible polymers poly (D, L-lactide)-co-(glycolide) (PLGA), polyethylene glycol (PEG), and polyvinyl pyrrolidone (PVP) on core-shell structures including silver nanoparticles that were activated with magnetic nanoparticles (MNPs). Emulsion solvent evaporation technique was employed to synthesize three types of shells: (i) (PVP-PEG) (100:20, w/w), (ii) (PLGA-PEG) (100:20, w/w), and (iii) (PLGA-PEG) (50:10, w/w) introduced as D1, D2, and D3 respectively. The in vitro release of AmB was examined in aqueous medium phosphate buffer saline (PBS) in pH~ 7.2. Several spectroscopy methods characterized the structure and properties of the nanoparticles. In vitro antifungal activity of pure AmB and D1, D2, and D3 was studied against *Candida albicans* (*C. albicans*). The results explained that frequency of drug released from D2 at the first 10 h was (18%) that was compared with D1 (30%) and D3 (24%) at the same time. D2 had more efficient and longer targeted controlled release. The findings showed that D2 can be used as an effective carrier for in vitro targeted controlled release and D2 and D3 had powerful activity against *C. albicans*.

Keywords Drug delivery · Amphotericin B · Magnetic nanoparticles · Core-shell · Emulsion solvent evaporation

Introduction

A drug delivery system (DDS) is an arrangement of formulations or devices that can bring a drug combination into the body and preserve the efficacy and safety of the medicine by administrating the speed, time, and location of release. It can be stated, DDS is a connector among the patient and the medicine that can be a drug formulation to treat

✉ Shahram Moradi Dehaghi
Shm_moradi@iau-tnb.ac.ir

[1] Department of Chemistry, Islamic Azad University, Tehran North Branch, Tehran, Iran

or a device to convey the drug. Drug systems play an essential role in the pharmacological effects of medications since they can be effective on how to release the drug and its speed, as well as the distribution of the medicine in the body and even adverse side effects. An effective drug delivery system ensures that the active medicine can be placed in its right place at the right time and can be effective when subjected to the environment [1, 2]. The drug delivery systems can be classified into two categories according to the different characteristics. One of the categorizations is based on the path of administration, which can be through the digestive, injectable, mucosal, pulmonary, and dermatological systems. The other categorization is based on the drug release mechanism including immediate release which is one of the most common releases, the modified release which is classified as a new drug delivery system, delayed release, an extended release which in some cases is classified into two categories, the standard release, and the controlled release [3, 4]. Nanoparticle-based drug delivery systems have been mostly used during the last few decades [5]. These structures can be regarded as very effective drug delivery systems due to controlling and slowing down the drug release, protecting the drug molecules, reducing the particle size smaller than the cells, passing through the biological barriers to deliver the drug to the target site, increasing the sustainability of the drugs in the bloodstream, targeted drug delivery, and biocompatibility which increase the therapeutic efficacy of the drug. Drug delivery using nano-carriers is the main cause to improve the therapeutic efficacy of the drug using encapsulated drugs [6]. The magnetic nanoparticles are one of the most important groups of the inorganic nano-carrier nanoparticles [7, 8]. Superparamagnetic iron oxide (SPIO) particles are important parts of drug delivery systems [8–10]. Maghemite (γ-Fe_2O_3) superparamagnetic nanoparticles and magnetite (Fe_3O_4) are the main magnetic nanoparticles (MNPs) used in drug delivery and medical applications [11]. Superparamagnetic properties of magnetic nanoparticles (MNPs) can help to keep medicine centralized, prevent its dispersal in the medium, and can be used in targeted and controlled release systems using an external magnetic field [8]. Organic nano-carriers include liposome, solid lipid nanoparticles, polymeric nanoparticles, polymeric micelles, dendrimers, polymerases, and hydrogel nanoparticles [7, 8, 12–15]. Polymers are the most mainly used materials to form the nanoparticles. The polymers used in controlled drug release should be biocompatible and non-toxic and have no dischargeable impurities [8, 12, 14, 16]. Physically, it should also include a decent structure and a half-life as desired. Polymers used to make polymeric nanoparticles can be synthetic or natural. Polymeric nanoparticles are often selected from biodegradable types [12, 14, 17]. High stability and the possibility of making them in large quantities cause polymeric nanoparticles to be selected and used more often. Polymeric nanoparticles combine many compounds including vesicles (nanocapsules) systems and matrix systems (nanospheres). In nanocapsules, the drug is hermetically sealed in a polymeric cavity [8, 12, 13]. Most of the used synthetic biodegradable polymers include poly (lactic acid) (PLA), poly (glycolic acid) (PGA), poly-cyanoacrylate (PCA), polycaprolactone (PCL), and poly (lactide)-co-(glycolide) (PLGA) [10, 15, 18]. Poly (lactide)-co-(glycolide) (PLGA) is one of the superlative and prominent biodegradable polymers to deliver the drug. PLGA is mostly considered recently due to (i) low systematic toxicity, (ii) easily excretion out of the body, (iii) conservation of drug from decay, (iv) bioavailability and biocompatibility, and (v) increased drug stability [19, 20]. One of the problems with biodegradable polymers as carriers is their quick drainage out of the bloodstream through phagocytosis [21, 22]. Using poly (ethylene glycol) (PEG)

prevents the mentioned withdrawal [23]. The following types of drugs are loaded in PLGA nanoparticles: hormones, dexamethasone, insulin (diabetes medication), haloperidol (an antipsychotic medication), and many anticancer drugs (doxorubicin, paclitaxel, and cisplatin) [19, 20, 24]. AmB is a strong antibiotic which is used to treat fungal infections which were isolated from the streptomyces species in 1955 [25]. AmB has polyene hydrocarbon chains as hydrophobic and polyhydroxyl chains as hydrophilic as shown in Fig. 1 [26]. Minor solubility of this drug in solvents (aqueous and organic) is due to the amphoteric nature of AmB [27]. AmB sodium deoxycholate (Fungizone®) is used as a parenteral formulated drug [28]. There are many side effects caused by this form [29, 30]. The results express that when AmB is conjugated with PEG [31] or PLGA [30, 32], there was an increased solubility in water, reduced toxicity, and increased effects compared with the other AmB formulation.

In this research, loading AmB on a core-shell structure where the core included Ag nanoparticles was examined. The Ag nanoparticles were activated and centralized by magnetic particles. The shell included three types of polymers such as PLGA, PVP, and PEG with different ratios, named as D1, D2, and D3 respectively. The purpose of using different polymers was to develop a targeted and controlled release. The effect of the selected polymers and their amount on the in vitro release rate of the AmB for parenteral delivery process with modified bioavailability and less toxicity was examined as well. Fourier Transform Infrared (FT-IR), X-ray diffraction (XRD), Scanning Electron Microscopy (SEM), and Transmission Electron Microscopy (TEM) analysis characterized the structure and the properties of the nanoparticles. Vibrating-Sample Magnetometer (VSM) was used to examine the superparamagnetic properties of magnetic nanoparticles (MNPs). Thermogravimetric analysis (TGA) was used to examine thermal decomposition of composites and polymers. In vitro drug release of AmB was studied in aqueous medium phosphate buffered saline (PBS) in pH~ 7.2 at room temperature (due to the use of the parenteral form of AmB, this research was conducted only in a neutral medium). Ultra Violet-Visible (UV-Vis) spectrometry was used to examine the release

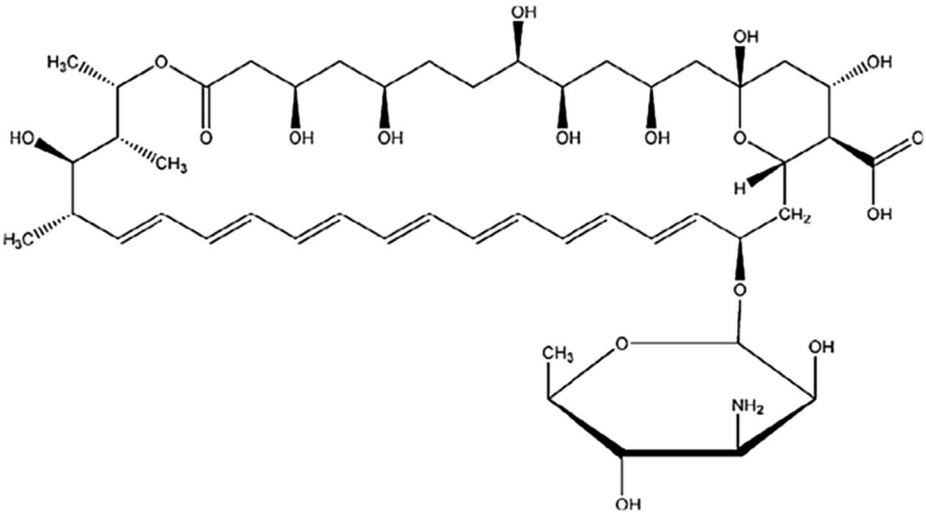

Fig. 1 Chemical structure of Amphotericin B (AmB) [26]

process. In vitro antifungal activity of pure AmB and AmB-loaded nanoparticles (D1, D2, and D3) was studied against *Candida albicans* (*C. albicans*).

Materials and Methods

Materials

AmB (101.26% assay, lyophilized bulk, for parenteral preparation) was purchased from Synbiotics Company. Poly (D, L-lactide-co-glycolide) (PLGA, 50:50, MW 40-75 kDa), sodium borohydride ($NaBH_4$, ≥ 98%), silver nitrate ($AgNO_3$, ≥ 99%), and citric acid (≥ 99.5%) were purchased from Sigma-Aldrich Company. Polyethylene glycol (PEG 6000, average mol wt 5000–7000), polyvinyl pyrrolidone (PVP), Sabouraud Dextrose Agar plates (SDA), Sabouraud Dextrose Broth 2%, ammonia (NH_3, 25%), sodium chloride, potassium chloride, $Na_2HPO_4.2H_2O$, KH_2PO_4, $Fe_3SO_4.7H_2O$, Fe $(NO_3)_3.9H_2O$, and polyethyleimine were purchased from Merck Chemical Company. Polyvinyl alcohol (PVA, 88% hydrolyzed) with Gohsenol Tradename was purchased from Nippon Gohsei. Analytical reagents used in this work: dimethyl sulfoxide (DMSO), dichloromethane, ethyl acetate, and deionized water were purchased from Merck Chemical Company.

Equipment

Thermo Nicolet 8700 FT-IR spectrophotometer used to obtain FT-IR spectra. UV-Vis absorption spectrum was obtained via Varian Carry 100 UV-Vis spectrometer. XRD patterns were obtained via a Philips X'Pert Pro MPD diffractometer with CuKα radiation from 10 to 80 (2θ) at room temperature. The results obtained from the Scanning Electron Microscope (SEM, TESCAN MIRA3) and Transmission Electron Microscopy (TEM, Philips EM 208 Electron Microscopy) showed the morphology and microanalysis of the nanoparticles. The data resulted from the Vibrating-Sample Magnetometer (VSM, Lakeshore 735) confirmed the superparamagnetic properties of the magnetic nanoparticles (MNPs). The data resulted from the Thermogravimetric analysis (TGA, SDT Q600 V20.9 Build 20) showed the thermal decomposition of nanoparticles and polymers.

Preparation of Magnetic Nanoparticles

The co-precipitation technique was used to produce magnetic nanoparticles (MNPs) [33, 41, 42]. In sum, $FeSO_4.7H_2O$ (4.2 g) and Fe $(NO_3)_3.9H_2O$ (8.6 g) were weighed and dissolved in 1000 mL water and the mixture was stirred for 1 h. 45 mL of ammonia (25%) was added and the mixture was stirred for 5 h. Then, 50 mL of citric acid (0.02 M) was added and sonicated at room temperature for 10 min. The solution was aged at room temperature for 24 h to form a precipitate, and the obtained precipitate was washed with purified water, then dried at 50 °C for 20 h.

Preparation of Ag Nanoparticles

The method employed in this reference was modified [34]. In sum, 300 mL of aqueous solution of 2.0×10^{-3} M sodium borohydride was added to 100 mL of aqueous solution of

1.0×10^{-3} M silver nitrate at 0 °C. In this process, Ag ions turned into Ag metal and a transparent sol of silver nanoparticle was produced in the medium. The process of stirring the solution was continued for 1 h for homogeneity and uniformity of the solution in darkness.

Preparation of Fe_3O_4-Ag Nanoparticles

The method employed in this reference was modified [42, 43]. The wet impregnation was used to add Ag to MNPs. In sum, silver nitrate was added to MNPs and this mixture was sonicated for 10 min. Then, the aqueous solution of 50% polyethyleimine was added to this mixture and sonicated at room temperature for 10 min. Produced mixture was filtered and the obtained precipitate was washed with alcohol and deionized water, then dried at 60 °C for 10 h.

Preparation of Phosphate Buffer Saline

Phosphate buffer saline (PBS) was provided according to the described instruction [35]. To prepare 1 L of PBS, NaCl (8.1 g), KCl (0.2 g), $Na_2HPO_4.2H_2O$ (1.78 g), and KH_2PO_4 (0.27 g) were dissolved in 800 mL of distilled water. The pH~ 7.2 was adjusted with HCl and the final volume was brought to 1 L. This solution was filtered through a filter paper to remove impurities.

Preparation of AmB-Loaded Nanoparticles

Nanoparticles were produced by an emulsion solvent evaporation technique [36]. At the first, AmB (0.1 g) was dissolved in 1 mL of DMSO and then it was added to 2 mL of an organic solvent containing dichloromethane and ethyl acetate (4:2, v/v). Certain amount of PVP-PEG (100:20, w/w) (also known as D1) was dissolved in dichloromethane. The amount of 0.011 g Fe_3O_4-Ag was added to this solution. The two prepared organic phases were mixed together. Final organic phases infused into 10 mL PVA (1%, w/v) and then the mixture was sonicated at room temperature for 10 min. Produced emulsion was subjected to evaporation under vacuum at 37 °C to produce the solid nanoparticles. Nanoparticles were separated by centrifugation and washed with deionized water. The nanoparticle precipitate was suspended in 5% sucrose and freeze-dried. The other nanoparticles PLGA-PEG (100:20, w/w) and PLGA-PEG (50:10, w/w) (also known as D2 and D3 respectively) were provided as the same method.

In Vitro Drug Release Study

The in vitro release test in this study was done based on the described instruction. The solution testing was performed on 20 mL of PBS in pH~ 7.2 at room temperature. Synthesized nanocapsules (0.2 g) containing 0.1 g lyophilized drug was dissolved in the medium. At certain time intervals (every 1 to 70 h), 5 mL of the sample was withdrawn from container and centrifuged for 5 min. UV-Vis spectrophotometry was used to analyze the supernatant solution. The testing solution was poured back into the container and kept at room temperature.

In Vitro Antifungal Study

Candida albicans (ATCC 90028) (*C. albicans*) was selected for examining the efficacy of AmB-loaded nanoparticles (D1, D2, and D3) and pure AMB. The broth dilution method was

used to determine the minimum inhibitory concentrations (MICs) of AMB in D1, D2, and D3 according to the National Committee for Clinical Laboratory Standard "NCCLS document M27-A, (Standards, 2002)". This is the most commonly used to test the susceptibility of microorganisms to antibiotics. In sum, *C. albicans* was diluted in Sabouraud Dextrose Broth 2% growth medium and 100 μL dispensed into board containing a concentration range of AMB 0.015–2 μg/mL. The board was incubated for 24 and 48 h at 32 °C. The *C. albicans* was grown on Sabouraud Dextrose Agar (SDA) and inoculated into Sabouraud Dextrose Broth 2%. The inoculated plates were incubated at 37 °C for 24 h [44, 45]. The growth colony was appraised oculary. The MIC was presented as the lowest AmB concentration that prevented visible growth of *C. albicans* and stated in μg/mL.

Result and Discussion

FT-IR Spectroscopy

FT-IR spectra of the nanoparticles, polymers, and AmB were obtained. Fig. 2 shows the results in the wave number range from 450 to 4000 cm^{-1}. The important peaks of AmB included the peak at 3390 cm^{-1} which can be attributed to stretching vibration of the O–H bond. The peak at 2940 cm^{-1} was attributed to the (C–H) CH_3 asymmetric stretching band. The sharp peak at 1691 cm^{-1} can be attributed to C=O stretch band and NH_2 in-plane bending vibration. The peak around 1567 cm^{-1} can be attributed to the stretching band of C=C of the polyene. The peak at 1402 cm^{-1} was attributed to the C–H bending vibration in polyene ring. The peak around 1068 cm^{-1} can be attributed to the asymmetric stretching vibration of C=O. The peak at 1009 cm^{-1} was attributed to the C–H bending out of plane bend (trans-polyene). The peak around 851 cm^{-1} can be attributed to the C–H bending vibration in pyranose ring

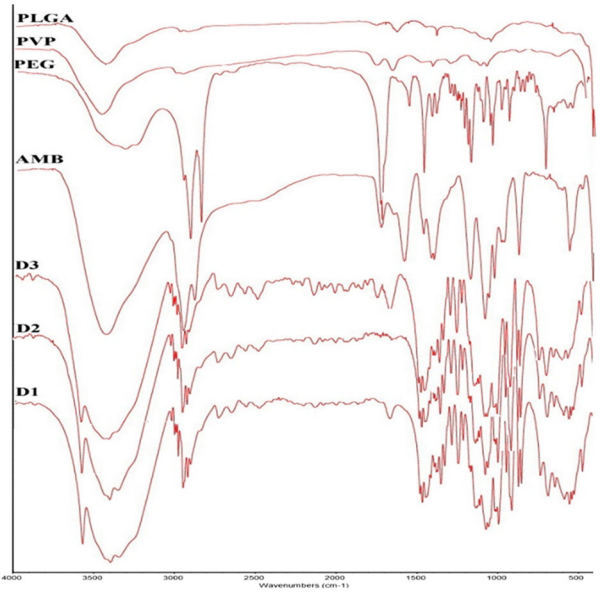

Fig. 2 FT-IR spectra of D1, D2, D3, AmB, PEG, PLGA, and PVP

vibration [32, 37]. The results showed that the IR spectrum of AmB was different from AmB-NPs. In freeze-dried samples of AmB-NPs, stretching vibration of C=O was lost because of the interaction between AmB and used polymers (D2) or it appeared less intense (D1 and D3). The peak at 1125 cm^{-1} was attributed to the new ether bond because of hydrogen bonding interplay among PLGA-PEG polymers and the carboxylic acid group of AmB [37]. The results confirmed that the interplay was completed between AmB and polymers and show successful addition of AmB and MNPs to PLGA-PEG and PVP-PEG polymers. The results show that the peak around 3392 cm^{-1} can be attributed highly to formed hydrogen bonding in freeze-dried samples of AmB-NPs.

SEM and TEM Analysis

The surface morphology of the Fe_3O_4-Ag and AmB-MNPs has been examined and Fig. 3 shows their SEM images. Fig. 3 a indicates that D1 (PVP and PEG) had an agglomeration and the approximate mean size of 62 nm. After loading AmB in the D3 and D2 (PLGA and PEG with different ratios), Fig. 3 b and c show that the mean particle size changed to 36 and 14 nm, respectively [38], and the dispersal of nanoparticles was improved. The images of these nanoparticles show minor agglomeration. Fig. 3 d indicates that Fe_3O_4-Ag had lower agglomeration and the approximate mean size of 20 nm.

Results obtained from TEM demonstrate the nanostructure of the AmB-MNPs as shown in Fig. 4. As the images show, the nanoparticles include clay-shaped particles whose tissues are not connected, and they are only discrete particles that are composed together.

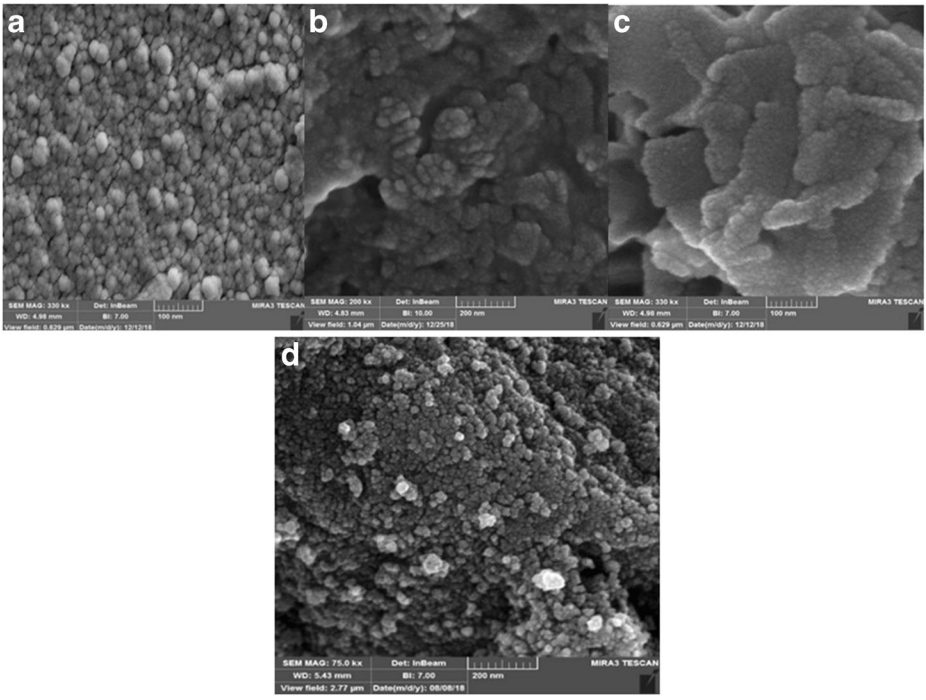

Fig. 3 SEM images for AmB-NPS containing 100 mg AmB and gathered with **a)** D1, **b)** D3, **c)** D2, and **d)** Fe_3O_4-Ag

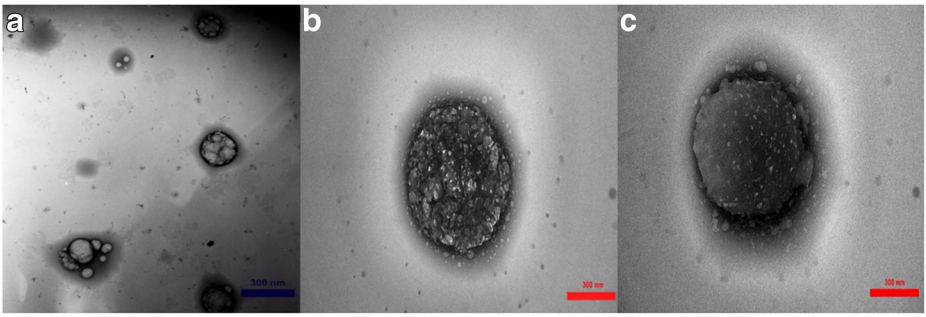

Fig. 4 TEM images for AmB-NPS containing 100 mg AmB and gathered with **a)** D1, **b)** D3, and **c)** D2

XRD

Fig. 5 shows the XRD patterns of Fe_3O_4 and Fe_3O_4-Ag. The XRD peaks at 2θ: 30°(220), 35.4°(311), 43°(400), 53.4°(422), 57°(511), and 62.6°(440), attributed to the Fe_3O_4 in the cubic lattice. Moreover, four peaks were observed at 2θ: 38°(111), 44°(200), 65°(220), and 77°(311), attributed to the Fe_3O_4-Ag [39].

VSM

VSM examined the superparamagnetic properties of magnetic nanoparticles (MNPs). D1, D2, and D3 were examined by this technique. Fig. 6 shows the obtained results. The magnetization of MNPs was examined in an applied magnetic field of $-10{,}000 \leq H$ (Oe) $\leq 10{,}000$ at room temperature. The result showed that there is a maximum oscillation in

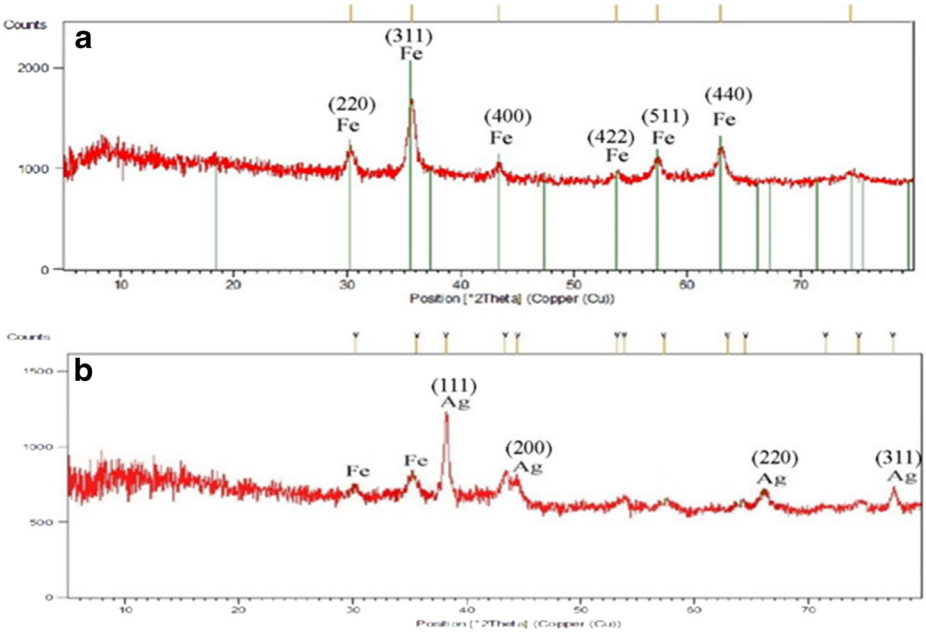

Fig. 5 XRD pattern of **a)** Fe_3O_4 and **b)** Fe_3O_4-Ag

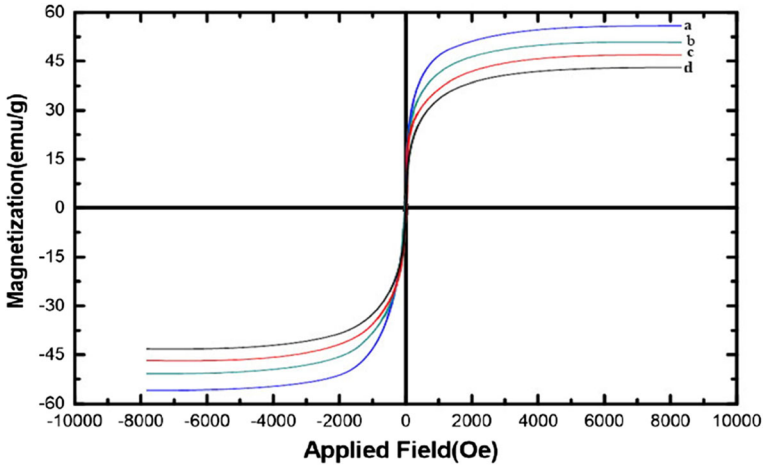

Fig. 6 VSM analysis for **a)** MNPs, **b)** D2, **c)** D3, and **d)** D1

the range between −4000 and 4000. This pattern confirms the superparamagnetic behavior of the nanoparticles. Conforming to VSM results, the highest magnetization that was equalized to 57 emu/g is related to MNPs. By loading the D2 and D3 shells (PLGA with different ratios), the magnetic behavior was reduced, with the D1 shell (PVP) founding 51, 47, and 39 emu/g, respectively. The amount of MNPs in the core of D1, D2, and D3 is fixed which is improved by TGA results. With changing the shells, the ratio of magnetic mass in the core is reduced to the total mass of nanoparticle. It can be stated, as increasing the particle size reduced the magnetic properties. The superparamagnetic particles were enclosed in the core-shell of a drug. Drug release will have a focused point state using an external magnetic field. Superparamagnetic particles are activated and absorbed into the magnetic field. This specification can be employed for barricading scatteredness of the drug and centralizing it in the desirable site. It can be stated, the presence of magnetic nanoparticle facilitates drug guidance to target cells in the physiological environment of the body and the drug focusing on the target. After applying the magnetic field, the accumulation of the components of the AmB nanoparticles (but not AmB itself) was found to be around the magnetic field in the container. However, such a process is more important and effective in clinical trials. But in this research, it was measured as an individual parameter.

TGA Interpretation

Thermogravimetric analysis was performed on D1, D2, and D3. This analysis was carried out in an air medium at a temperature range of 25 to 800 °C. The increasing temperature rate was applied one degree every ten minutes.

The result showed that in D1, the weight loss of AmB was found to be about 45% at a temperature range of 180–261 °C. In the temperature range of 261–318 °C, 15% of the decreased weight was observed that is related to the weight loss of the PEG 6000. In the range of 318–382 °C, the 12% of thermal degradation was attributed to PVA. The next weight loss was 25% of the weight of the composite in the temperature range of 400–520 °C related to

PVP. Less than 2% of the weight of the composite remained that was related to the magnetic iron oxide.

In D2, the weight loss of AmB was about 6% at a temperature range of 170–210 °C. In the temperature range of 210–260 °C, 31% of weight loss was observed that is related to the weight loss of the PEG 6000. In the range of 260–390 °C, the thermal degradation was related to PVA that contained about 30% of the polymer. The next weight loss was in the temperature range of 390–530 °C related to PLGA that constituted about 29% of the weight of the composite. Less than 2% of the composite weight remained that was related to the magnetic iron oxide.

In D3, the weight loss of AmB was about 12% at a temperature range of 170–210 °C. In the temperature range of 210–270 °C, 30% of the weight loss was observed that is related to the weight loss of the PEG 6000. In the range of 270–370 °C, thermal degradation was related to PVA that consists of about 21% of the polymer. The next weight loss was in the temperature range of 370–500 °C related to PLGA that constituted about 32% of the weight of the composite. Less than 2% of the weight of composite remained that is related to the magnetic iron oxide (Figs. 7, 8, and 9).

In Vitro Release of Amphotericin B

The in vitro drug release of AmB was examined in PBS [40]. This study was conducted in room temperature and in neutral environments with pH~ 7.2. This condition was selected for release studies because the solubility of AmB at low pH is severely reduced, so the exact amount of release cannot be measured. It can be stated, AmB is insoluble in acidic pH. The efficacy of drug carriers and rate of release in acidic pH was increased [32], but due to insolubility of AmB in acidic pH, the results were unrealistic. Fig. 10 shows the release rate for 70 h. Release results showed a biphasic release of AmB from the NPs [37]. In the first stage (10 h), there was a basic rapid release about 18–30% conforming to the ratios of polymers (D1, D2, and D3) followed by a gradual release stage from 10 to 70 h in which 9–12% of the drug was released. There was no time that shows a burst in drug release within the first 10 h of the

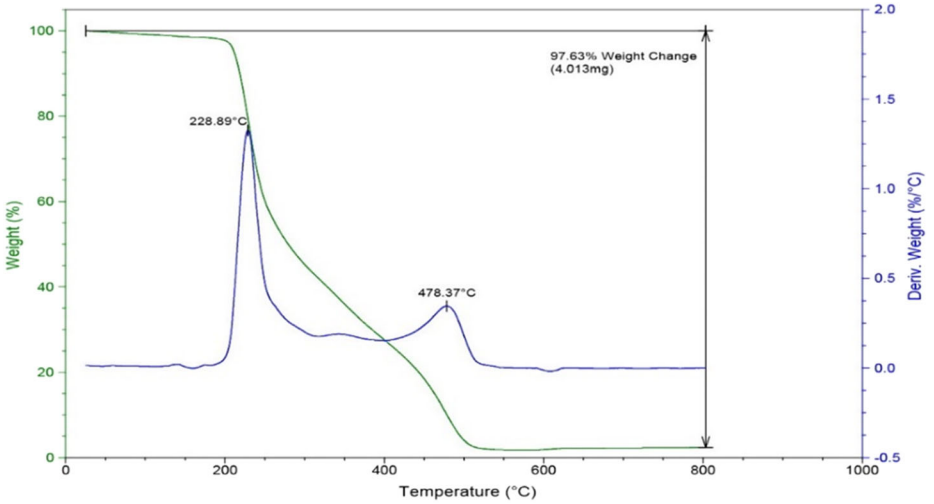

Fig. 7 TGA curve of D1

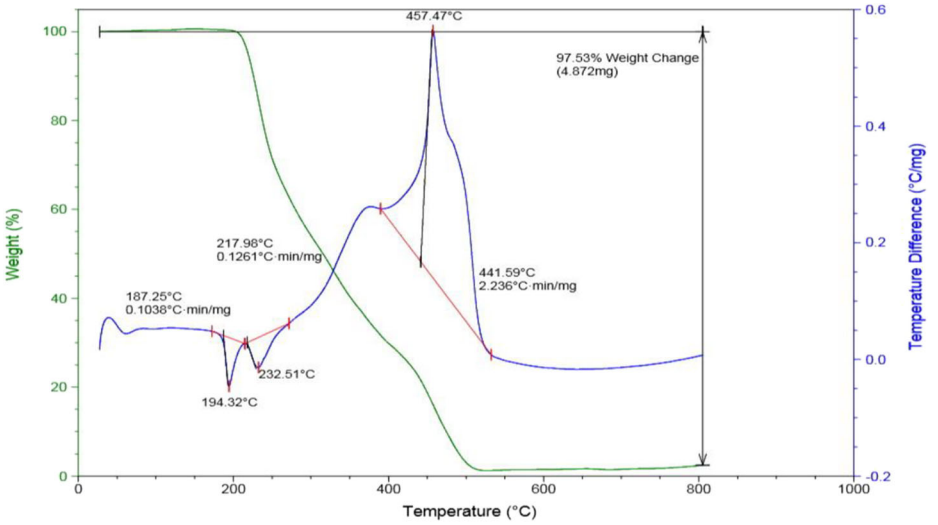

Fig. 8 TGA curve of D2

loaded AmB on the NPs that confirmed the obtained results. There is a maximum release rate in the first 10 h. Between 10 and 20 h, there was an increase in the release rate with a slight slope. After 20 h, there was a sustained release up to 70 h. The maximum drug release during 70 h was achieved with D1 (42%) and the lowermost was D2 (27%). Hence, the increase in the release rate in D2 is very mild and continuous, but it is almost constant in D1 after 20 h and its release is insignificant. In D3, after 30 h of reducing the rate of drug release, the results indicate drug re-absorption by polymers. The first stage of release took place maybe due to the dissolution and dissemination of AmB that was inadequately ensnared in the NPs. Whenever the slower and sustained release was being observed, it could be attributed to the dissemination of AmB localized in the core of NPs. Using the polymers owning linking ability to drugs such as PLGA that contain free carboxylic groups has lowered the burst release, but in some cases,

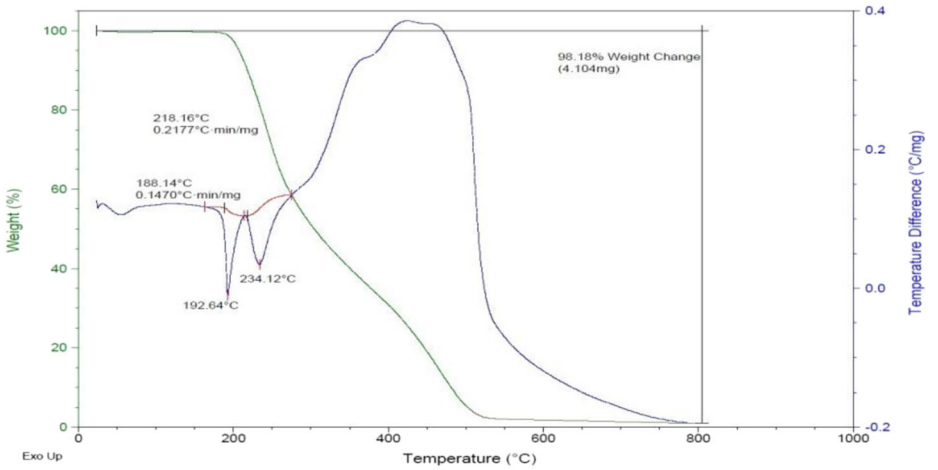

Fig. 9 TGA curve of D3

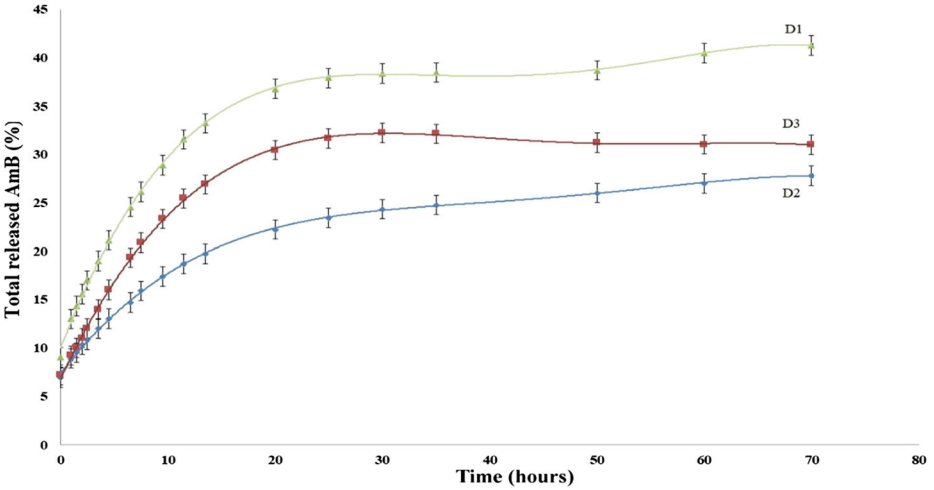

Fig. 10 In vitro drug release manner for AmB-NPs (error bars are mean ± SD, $n = 5$)

it stops or significantly prolongs the drug release. It also has specific features as the residual particles of this nanomedicine can degrade inside the body and convert into the basic compounds essential for the body. It can be assumed in the mechanism of drug release of AmB that AmB-NPs own major hydrophilicity, leading to a major tendency for the medium to diffuse into the core of nanoparticles inducing its swelling [37]. Therefore, from 0.1 g of AmB-loaded nanoparticles, according to TGA results, 45% (0.045 g), 6% (0.006 g), and 12% (0.012 g) and in vitro release of Amphotericin B after the end of 70 h showing 42% (0.0189 g), 27% (0.0016 g), and 32% (0.0038 g) were founded that is related to D1, D2, and D3 respectively.

In Vitro Antifungal Study

Table 1 presents the antimicrobial activity of pure AmB and AmB-loaded nanoparticles (D1, D2, and D3) in *C. albicans* after 24 and 48 h. The end-point (MIC-0) was reached for pure AmB 0.5 μg/mL and 1.0 μg/mL after 24 and 48 h respectively. The MIC-0 for AMB in D2 and D3 (AmB-loaded to PLGA-PEG) was reduced more than D1 (AmB-loaded to PVP-PEG). The MIC of AmB in D2 and D3 was reduced against *C. albicans* compared with free AmB more than fourfold. Hence, AmB-loaded to PLGA-PEG (D2 and D3) have high efficacy and are very effective for treatment of fungal infections containing *C. albicans*.

Table 1 Antifungal activity of AmB against *C. albicans* ($n = 5$)

Tested form	MIC-0 (μg/mL) after 24 h	MIC-0 (μg/mL) after 48 h
AmB	0.5 ± 0.01	1.0 ± 0.01
D1	0.225 ± 0.01	0.225 ± 0.01
D2	0.115 ± 0.01	0.115 ± 0.01
D3	0.115 ± 0.01	0.115 ± 0.01

Conclusion

Generally, it is deserving to say, the selected polymers and their amount showed that they are effective parameters controlling the rate of drug release. The results explained that adding PVP (D1) significantly increases the in vitro release compared with the other formulations. This can be attributed to the low molecular mass and high solubility of PVP. The drug release can be done slowly in the presence of PLGA in (D2 and D3) polymers due to its high molecular mass and its reducing solubility in physiological media. Simultaneously used PLGA and PEG with the same applying percentage can be effective in increasing and decreasing the drug release rate. The selected PLGA and PEG with (100:20, w/w) ratio indicated a controlled release rate for a longer period of time. The results indicated that selected polymers with different amounts prolonged drug release process for a specific dose of parenteral AmB interval of 10 to 20 h. D1 as a carrier is proper for these cases where the maximum release of the AmB is required in a controlled period at 10 h. D2 as a carrier is proper for slow controlled drug release for a 20 h or a long period of time. These results express that oral AmB is still the first-line treatment in cases where a high dose is required in a very short period of time. PLGA as a biodegradable and biocompatible polymer can be used as a suitable substrate to load high volumes of parenteral AmB. The result of the in vitro antifungal study indicated that AmB-loaded to PLGA-PEG (D2 and D3) have powerful activity against *C. albicans*.

Compliance with Ethical Standards

Conflict of Interest The authors declare that they have no conflict of interest.

References

1. Jain, K. K. (2008). *Drug delivery systems*. Totowa, USA: Humana.
2. Nabipour, H. (2019). Design and evaluation of non-steroidal anti-inflammatory drug intercalated into layered zinc hydroxide as a drug delivery system. *Journal of Inorganic and Organometallic Polymers, 29*(5), 1807–1817. https://doi.org/10.1007/s10904-019-01143-x.
3. Saltzman, W. M. (2001). *Drug delivery engineering principles for drug therapy*. USA: Oxford Press.
4. Perrie, Y., & Redes, T. (2012). *FASTtrack: pharmaceutics-drug delivery and targeting* (second ed.). USA: Pharmaceutical Press.
5. Yun, Y. H., Lee, B. K., & Park, K. (2015). Controlled drug delivery: historical perspective for the next generation. *Journal of Controlled Release, 219*, 2–7. https://doi.org/10.1016/j.jconrel.2015.10.005.
6. Benita, S. (2006). *Microencapsulation methods and industrial application* (2nd ed.). Boca Raton, USA: CRC.
7. De Villiers, M. M., Aramwit, P., & Kwon, G. S. (2008). *Nanotechnology in drug delivery*. USA: AAPS.
8. Arias, J. L. (2014). *Nanotechnology and drug delivery* (Vol. 1: Nanoplatforms in Drug Delivery). USA: CRC.
9. Wahajuddin, S. A. (2012). Superparamagnetic iron oxide nanoparticle: magnetic nanoplatforms as drug carriers. *International Journal of Nanomedicine, 7*, 3445–3471. https://doi.org/10.2147/IJN.S30320.
10. Lee, J. H., Kim, J. W., & Cheon, J. (2013). Magnetic nanoparticles for multi-imaging and drug delivery. *Molecules and Cells, 35*(4), 274–284. https://doi.org/10.1007/s10059-013-0103-0.
11. Figuerola, A., Di Corato, R., Manna, L., & Pellegrino, T. (2010). From iron oxide nanoparticle towards advanced iron-based inorganic materials designed for biomedical applications. *Pharmacological Research, 62*(2), 126–143. https://doi.org/10.1016/j.phrs.2009.12.012.
12. Mishra, A. K. (2013). *Nanomedicine for drug delivery and therapeutics*. USA: Wiley.
13. Kaparissides, C., Alexandridou, S., Kotti, K., & Chaitidou, S. (2006). Recent advanced in novel drug delivery systems. *Journal of Nanotechnology, 2*, 1–11. https://doi.org/10.2240/azojono0111.

14. Yashwant, P. (2016). Recent developments in nanoparticulate drug delivery systems. In Y. Pathak & D. Thassu (Eds.), *Drug delivery nanoparticles formation and characterization* (pp. 1–15). New York: Informa Healthcare Inc.
15. Kamaly, N., Yameen, B., Wu, J., & Farokhzad, O. C. (2016). Degradable controlled-release polymers and polymeric nanoparticles: mechanisms of controlling drug release. *Chemical Reviews, 116*(4), 2602–2663. https://doi.org/10.1021/acs.chemrev.5b00346.
16. Singh, R., & Lillard Jr., J. W. (2009). Nanoparticle-based targeted drug delivery. *Experimental and Molecular Pathology, 86*(3), 215–223. https://doi.org/10.1016/j.yexmp.2008.12.004.
17. D'Mello, R. S., Das, K. P., & Das, N. G. (2016). Polymeric nanoparticles for small-molecule drugs: biodegradation of polymers and fabrication of nanoparticles. In Y. Pathak & D. Thassu (Eds.), *Drug delivery nanoparticles formation and characterization* (pp. 16–34). New York: Informa Healthcare Inc.
18. Parveen, S., & Sahoo, S. K. (2008). Polymeric nanoparticles for cancer therapy. *Journal of Drug Targeting, 16*(2), 108–123. https://doi.org/10.1080/10611860701794353.
19. Danhier, F., Ansorena, E., Silva, J. M., Coco, R., Breton, A. L., & Preat, V. (2012). PLGA-based nanoparticles: an overview of biomedical applications. *Journal of Controlled Release, 161*(2), 505–522. https://doi.org/10.1016/j.jconrel.2012.01.043.
20. Kumari, A., Yadav, S. K., & Yadav, S. C. (2010). Biodegradable polymeric nanoparticles based drug delivery systems. *Colloids and Surfaces. B, Biointerfaces, 75*(1), 1–18. https://doi.org/10.1016/j.colsurfb.2009.09.001.
21. Stolink, S., Illum, L., & Davis, S. S. (1995). Long circulating microparticulate drug carriers. *Advanced Drug Delivery Reviews, 16*(2–3), 195–214. https://doi.org/10.1016/0169-409X(95)00025-3.
22. Owens III, D. E., & Peppas, N. A. (2006). Opsonization, biodistribution, and pharmacokinetics of polymeric nanoparticles. *International Journal of Pharmaceutics, 307*(1), 93–102. https://doi.org/10.1016/j.ijpharm.2005.10.010.
23. Jee, J.-P., McCoy, A., & Mecozzi, S. (2012). Encapsulation and release of amphotericin B from an ABC triblock fluorous copolymer. *Pharmaceutical Research, 29*(1), 69–82. https://doi.org/10.1007/s11095-011-0511-9.
24. Reis, C. P., Neufeld, R. J., Ribeiro, A. J., & Veiga, F. (2006). Nanoencapsulation I. Methods for preparation of drug-loaded polymeric nanoparticles. *Nanomedicine: Nanotechnology, Biology and Medicine, 2*(1), 8–21. https://doi.org/10.1016/j.nano.2005.12.003.
25. Wu, T. C. (1994). On the development of antifungal agents: perspective of the U.S. Food and Drug Administration. *Clinical Infectious Disease, 19*(Suppl.1), S54–S58. https://doi.org/10.1093/clinids/19.supplement_1.s54.
26. Zu, Y., Sun, W., Zhao, X., Wang, W., Li, Y., Ge, Y., Liu, Y., & Wang, K. (2014). Preparation and characterization of amorphous amphotericin B nanoparticles for oral administration through liquid antisolvent precipitation. *European Journal of Pharmaceutical Sciences, 53*, 109–117. https://doi.org/10.1016/j.ejps.2013.12.005.
27. Ménez, C., Legrand, P., Rosilio, V., Lesieur, S., & Barratt, G. (2007). Physicochemical characterization of molecular assemblies of miltefosine and amphotericin B. *Molecular Pharmaceutics, 4*(2), 281–288. https://doi.org/10.1021/mp0601143.
28. Dutcher, J. D. (1968). The discovery and development of amphotericin B. *Diseases of the Chest, 54*(Suppl.1), 296–298. https://doi.org/10.1378/chest.54.supplement_1.296.
29. Torrado, J. J., Espada, R., Ballesteros, M. P., & Torrado-Santiago, S. (2008). Amphotericin B formulations and drug targeting. *Journal of Pharmaceutical Sciences, 97*(7), 2405–2425. https://doi.org/10.1002/jps.21179.
30. Van de Ven, H., Paulussen, C., Feijens, P. B., Matheeussen, A., Rombaut, P., Kayaert, P., Van den Mooster, G., Weyenberg, W., Cos, P., Maes, L., & Ludwing, A. (2012). PLGA nanoparticles and nanosuspensions with amphotericin B: potent in vitro and in vivo alternatives to Fungizone and AmBisome. *Journal of Controlled Release, 161*(3), 795–803. https://doi.org/10.1016/j.jconrel.2012.05.037.
31. Conover, C. D., Zhao, H., Longley, C. B., Shum, K. L., & Greenwald, R. B. (2003). Utility of poly (ethylene glycol) conjugation to create prodrugs of amphotericin B. *Bioconjugate Chemistry, 14*(3), 661–666. https://doi.org/10.1021/bc0256594.
32. Nahar, M., & Jain, N. K. (2009). Preparation, characterization and evaluation of targeting potential of amphotericin B-loaded engineered PLGA nanoparticles. *Pharmaceutical Research, 26*(12), 2588–2598. https://doi.org/10.1007/s11095-009-9973-4.
33. Khalafalla, S., & Reimers, G. (1980). Preparation of dilution-stable aqueous magnetic fluids. *IEEE Transactions on Magnetics, 16*(2), 178–183. https://doi.org/10.1109/TMAG.1980.1060578.
34. Kim, J. S., Kuk, E., Yu, K. N., Kim, J. H., Park, S. J., Lee, H. J., Kim, S. H., Park, Y. K., Park, Y. H., Hwang, C.-Y., Kim, Y.-K., Lee, Y. S., Jeong, D. H., & Cho, M.-H. (2007). Antimicrobial effects of silver

nanoparticles. *Nanomedicine: Nanotechnology, Biology and Medicine, 3*(1), 95–101. https://doi.org/10.1016/j.nano.2006.12.001.
35. Morris, M. C., Depollier, J., Merry, J., & Heitz, F. (2001). A peptide carrier for the delivery of biologically active proteins into mammalian cells. *Nature Biotechnology, 19*(12), 1173–1176. https://doi.org/10.1038/nbt1201-1173.
36. Carraro, T. C. M. M., Khalil, N. M., & Mainardes, R. M. (2016). Amphotericin B-loaded polymeric nanoparticle: formulation optimization by factorial design. *Pharmaceutical Development and Technology, 21*(2), 140–146. https://doi.org/10.3109/10837450.2014.979942.
37. AL-Quadeib, B. T., Radwan, M. A., Šiller, L., Horrocks, B., & Wright, M. C. (2015). Stealth amphotericin B for oral drug delivery: in vitro optimization. *Saudi Pharmaceutical Journal, 23*(3), 290–302. https://doi.org/10.1016/j.jsps.2014.11.004.
38. Taatabaei Mirakabad, F. S., Akbarzadeh, A., Milani, M., Zarghami, N., Taheri-Anganeh, M., Zeighamian, V., Badrzadeh, F., & Rahmati-Yamchi, M. (2016). A comparison between the cytotoxic effects of pure curcumin and curcumin-loaded PLGA-PEG nanoparticles on the MCF-7 human breast cancer cell line. *Artificial Cells, Nanomedicine, and Biotechnology, 44*(1), 423–430. https://doi.org/10.3109/21691401.2014.955108.
39. Yang, Y., Ren, S., Zhang, X., Yu, Y., Liu, C., Yang, J., & Miao, L. (2018). Safety and efficacy of PLGA (Ag- Fe_3O_4)-coated dental implants in inhibiting bacteria adherence and osteogenic inducement under a magnetic field. *International Journal of Nanomedicine, 13*, 3751–3762. https://doi.org/10.2147/IJN.S159860.
40. Choi, K. C., Bang, J. Y., Kim, P. I., Kim, C., & Song, C. E. (2008). Amphotericin B-incorporated polymeric micelles composed of poly (D, L-lactide-co-glycolide)/dextran graft copolymer. *International Journal of Pharmaceutics, 355*(1–2), 224–230. https://doi.org/10.1016/j.ijpharm.2007.12.011.
41. Kesavan, M. P., Kotla, N. G., Ayyanaar, S., Kumar, R. G., Sivaraman, G., Webster, T. J., & Rajesh, J. (2018). A theranostic nanocomposite system based on iron oxide-drug nanocages for targeted magnetic field responsive chemotherapy. *Nanomedicine: Nanotechnology, Biology and Medicine, 14*(5), 1643–1654. https://doi.org/10.1016/j.nano.2018.04.013.
42. Hong, S., Li, Z., Li, C., Dong, C., & Shuang, S. (2018). β-Cyclodextrin grafted polypyrrole magnetic nanocomposites toward the targeted delivery and controlled release of doxorubicin. *Applied Surface Science, 427*, 1189–1198. https://doi.org/10.1016/j.apsusc.2017.08.201.
43. Pachla, A., Lendzion-Bieluń, Z., Moszyński, D., Markowska-Szczupak, A., Narkiewicz, U., WrÓbel, R. J., Guskos, N., & Żołnierkiewicz, G. (2016). Synthesis and antibacterial properties of Fe_3O_4-Ag nanostructures. *Polish Journal of Chemical Technology, 18*(4), 110–116. https://doi.org/10.1515/pjct-2016-0079.
44. Radwan, M. A., AL-Quadeib, B. T., Šiller, L., Wright, M. C., & Horrocks, B. (2017). Oral administration of amphotericin B nanoparticles: antifungal activity, bioavailability and toxicity in rats. *Drug Delivery, 24*(1), 40–50. https://doi.org/10.1080/10717544.2016.1228715.
45. Jung, S. H., Lim, D. H., Jung, S. H., Lee, J. E., Jeong, K.-S., Seong, H., & Shin, B. C. (2009). Amphotericin B-entrapping lipid nanoparticles and their in vitro and in vivo characteristics. *European Journal of Pharmaceutical Sciences, 37*(3–4), 313–320. https://doi.org/10.1016/j.ejps.2009.02.021.